Colossal magnetoresistance and topological phase transition in $EuZn_2As_2$

Shuaishuai Luo,[1] Yongkang Xu,[1] Feng Du,[1] Lin Yang,[2] Yuxin Chen,[1] Chao Cao,[1,3] Yu Song,[1,3,*] and Huiqiu Yuan[1,3,4,5,†]

[1]*Center for Correlated Matter and School of Physics, Zhejiang University, Hangzhou 310058, China*

[2]*College of Materials and Environmental Engineering, Hangzhou Dianzi University, Hangzhou 310018, China*

[3]*Zhejiang Province Key Laboratory of Quantum Technology and Device, School of Physics, Zhejiang University, Hangzhou 310058, China*

[4]*State Key Laboratory of Silicon Materials, Zhejiang University, Hangzhou 310058, China*

[5]*Collaborative Innovation Center of Advanced Microstructures, Nanjing 210093, China*

(Received 4 May 2023; revised 23 September 2023; accepted 31 October 2023; published 17 November 2023)

We report electrical transport properties of $EuZn_2As_2$ under pressures up to 26 GPa. At ambient pressure, $EuZn_2As_2$ exhibits an insulating ground state and a ≈200% negative magnetoresistance (MR) at $B = 5$ T and $T = 2$ K. For pressures up to ∼3 GPa, the system becomes more insulating, accompanied by a dramatic enhancement of the MR ($B = 5$ T and $T = 2$ K) up to ≈14 000%. Further increase of pressure drives $EuZn_2As_2$ into a metallic state without significant MR. Resistivity measurements under field reveal ferromagnetic characteristics associated with the metallic ground state in pressurized $EuZn_2As_2$, distinct from the antiferromagnetic state realized at ambient pressure. We propose the pressure-induced insulator-metal transition and the colossal MR both originate from transformations of the magnetic ground state that strongly reconstruct the electronic structure. This view is supported by first-principles calculations, which further reveal that while antiferromagnetic $EuZn_2As_2$ is a trivial insulator, spin-polarized/ferromagnetic $EuZn_2As_2$ is a Weyl metal, indicting that the insulator-metal transition in $EuZn_2As_2$ is also a topological phase transition. These pressure- and field-induced topological phase transitions in $EuZn_2As_2$ are remarkably similar to behaviors reported in $EuCd_2As_2$, suggesting a common origin. Our findings demonstrate that spin-orbit coupling, electronic topology, and particularly the magnetic ground state play key roles in determining the physical properties of Eu-based magnetic topological materials.

DOI: 10.1103/PhysRevB.108.205140

I. INTRODUCTION

Large negative magnetoresistance (MR) is widely observed in doped manganites and is commonly referred to as colossal magnetoresistance (CMR) [1,2]. Similar large negative MR has been reported in many Eu-based compounds, and several possible CMR mechanisms have been proposed, including insulator-metal transitions [3–7], magnetic fluctuations [8–10], magnetic polarons or ferromagnetic clusters that localize carriers [11–14], and Berezinskii-Kosterlitz-Thouless (BKT) transitions [15,16]. Although there appears to be no universal mechanism for the generation of CMR in Eu-based compounds, Eu magnetism is clearly a key component.

With recent developments in magnetic topological states of matter, in which electronic topology depends on both the crystalline and magnetic symmetries [17–24], it has been found that nearly degenerate magnetic states can correspond to distinct topological phases [25–35]. In such cases, the alteration of magnetic structures could lead to topological phase transitions, and the corresponding changes in physical properties open up a pathway towards realizing functional properties such as CMR. A prime example of this is realized in $EuCd_2As_2$, which at ambient pressure exhibits an antiferromagnetic (AFM) ground state with moments in the *ab* plane [36]. Theoretical calculations suggest ambient-pressure $EuCd_2As_2$ is a magnetic topological insulator (MTI) in the AFM state and a Weyl semimetal (WSM) in the polarized state [27,28].

Metallic transport is observed in both the MTI and WSM phases of $EuCd_2As_2$ [35–38], with metallic surface states or inadvertent doping possibly contributing to metallic conduction in the MTI phase. With the application of pressure that suppresses band inversion, $EuCd_2As_2$ changes from a MTI to a trivial insulator (TrI) at around 1.0 GPa, and the electrical transport changes from metallic to insulating [35]. By polarizing the spins in the TrI phase with an applied magnetic field, $EuCd_2As_2$ becomes a WSM and results in a CMR of up to 10^5% ($B = 0.22$ T and $T = 0.3$ K). With further increase of pressure to around 2.0 GPa, the magnetic state of $EuCd_2As_2$ changes from AFM to ferromagnetic (FM), and the associated electronic structure reconstruction leads to an insulator-metal transition (TrI to WSM). The consecutive topological phase transitions in pressurized $EuCd_2As_2$ lead to an insulating dome within the small pressure range between ≈1.0 and ≈2.0 GPa, which hosts the CMR effect [35].

To investigate how the topological phase transitions and CMR in $EuCd_2As_2$ may be affected by tuning via elemental substitution, it is instructive to study analog materials with the same trigonal $CaAl_2Si_2$-type structure [39–45]. In the case of $EuZn_2As_2$, the replacement of Cd with Zn leads to

*yusong_phys@zju.edu.cn

†hqyuan@zju.edu.cn

positive chemical pressure and a weakened spin-orbit coupling, both strongly affecting whether a material is topologically nontrivial. At ambient pressure, $EuZn_2As_2$ exhibits the same A-type AFM (A-AFM) order as in $EuCd_2As_2$, but with a higher Néel temperature, $T_N \approx 19$ K [9,10,46]. In contrast to $EuCd_2As_2$, which is topologically nontrivial at ambient pressure, first-principles calculations at ambient pressure show a topologically trivial narrow band gap in $EuZn_2As_2$, and a MR up to 200% well inside the A-AFM state is found experimentally [9]. These findings suggest $EuZn_2As_2$ at ambient pressure may correspond to the TrI phase in pressurized $EuCd_2As_2$ and motivates further detailed studies.

In this work we report electrical transport measurements and first-principles calculations in pressurized $EuZn_2As_2$. It is found that the insulating ground state persists up to ~3 GPa, with the most insulating state and a maximum CMR of 14 000% ($B = 5$ T and $T = 2$ K) observed at 1.6 GPa. Above a threshold pressure p_c, occurring between 2.9 and 3.9 GPa, the ground state of $EuZn_2As_2$ becomes metallic, which then persists up to at least 26 GPa. Electrical transport in applied fields suggests the metallic ground state exhibits FM order, or a state with a significant FM component (FM-like). Our experimental observations suggest that both the pressure-induced insulator-metal transition and the CMR effect originate from changes in the magnetic ground state, further supported by first-principles calculations. Moreover, our calculations reveal that while the insulating state of $EuZn_2As_2$ is topologically trivial, the metallic state exhibits Weyl fermions and Fermi arcs, evidencing the pressure- or field-induced insulator-metal transition to be a topological phase transition. These findings in $EuZn_2As_2$ are similar to behaviors in $EuCd_2As_2$, and demonstrate that the intersection of magnetism and electronic topology can give rise to tunable topological phase transitions and functional physical properties.

II. METHODS

Single crystals of $EuZn_2As_2$ were grown using Sn flux [9,10,47]. Energy-dispersive x-ray spectroscopy (EDS) measurements indicate the Eu:Zn:As atomic ratio in our samples is 19.65%:40.04%:40.31%, suggesting that the sample stoichiometry is close to the nominal 1:2:2, with no detectable Sn flux. Physical property measurements were performed using a Quantum Design PPMS. At ambient pressure, electrical resistivity was measured with the standard four-point method. Magnetization and magnetic susceptibility were measured using the VSM option of the PPMS. Electrical resistivity measurements under pressure were conducted in a diamond anvil cell (DAC) using the van der Pauw method, with Daphne oil 7373 as the pressure transmitting medium. Pressure values inside the DAC were determined using the ruby fluorescence method at room temperature. In all resistivity measurements, the current is in the *ab* plane and applied fields are along the *c* axis.

First-principles calculations were carried out in the framework of the generalized gradient approximation (GGA) with Perdew-Burke-Ernzerhof (PBE) functionals [48] using the VASP package [49]. The GGA + U method with $U = 5$ eV was applied to describe the valence $4f$ orbitals of the Eu atoms. The lattice parameters and internal atomic coordinates were optimized at each pressure such that the forces on each atom were smaller than 0.01 eV/Å. The maximally projected Wannier functions were constructed using the WANNIER90 code [50] and symmetrized by WANNSYMM [51]. Surface states were calculated using WANNIERTOOLS [52].

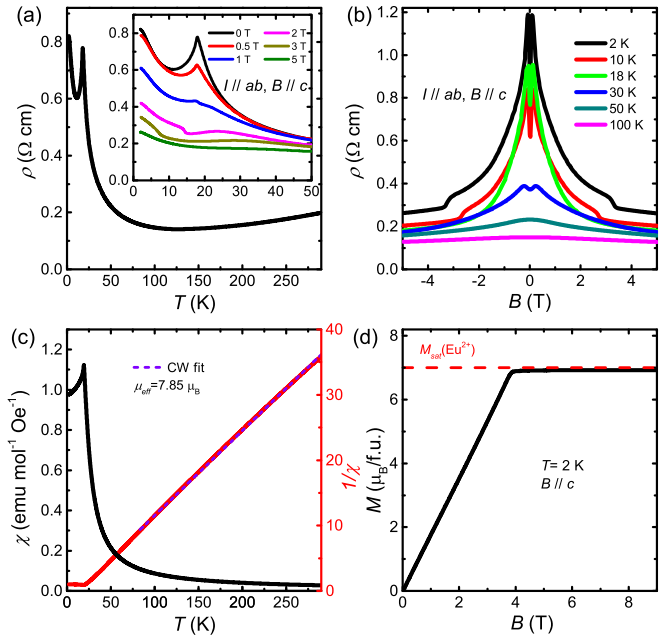

FIG. 1. Characterizations of $EuZn_2As_2$ at ambient pressure. (a) Temperature dependence of electrical resistivity $\rho(T)$ at zero field. The inset zooms in around T_N and also shows the evolution of $\rho(T)$ under various *c*-axis fields. (b) Field dependence of the resistivity at different temperatures, with fields applied along the *c* axis. (c) Magnetic susceptibility and its inverse, with the dashed line a Curie-Weiss fit for the high-temperature data. (d) Magnetization at 2 K with fields along the *c* axis, with the red dashed line showing the saturated moment for a fully localized Eu^{2+} ion.

III. RESULTS

A. Physical properties at ambient pressure

Figure 1 summarizes the physical properties of $EuZn_2As_2$ at ambient pressure. An AFM transition is signaled by a sharp peak at around 18 K in both resistivity $\rho(T)$ [Fig. 1(a)] and magnetic susceptibility [Fig. 1(c)]. The inset of Fig. 1(a) zooms in around the transition temperature T_N, compared with $\rho(T)$ under various *c*-axis magnetic fields. With increasing field, a rapid decrease of resistivity is induced, in addition to the suppression of T_N expected for an AFM state. The large negative MR can also be seen through the evolution of the resistivity with applied field at fixed temperatures $\rho(B)$, as shown in Fig. 1(b). At small fields ($B \lesssim 1.0$ T), $\rho(B)$ is M-shaped for temperatures up to 30 K, consistent with previous reports of $EuZn_2As_2$, and may be related to impurity carriers [9,10,46,53].

Magnetization measurements at 2 K reveal a saturated moment of 6.93 μ_B/Eu [Fig. 1(d)] with a saturation field of 3.9 T, and Curie-Weiss fitting of the magnetic susceptibility at high temperatures gives an effective moment of 7.85 μ_B/Eu [Fig. 1(c)], both in good agreements with the expected

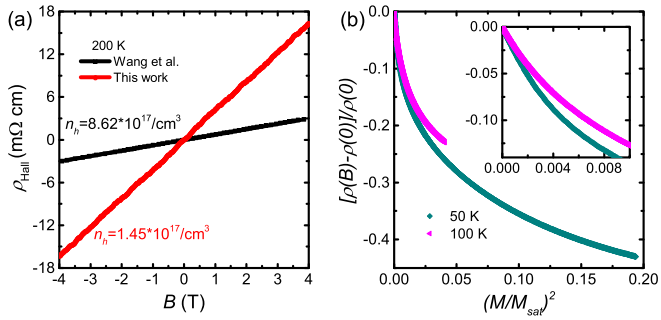

FIG. 2. (a) Comparison of the Hall resistivity at 200 K between samples in this work and in Ref. [9]. (b) $[\rho(B) - \rho(0)]/\rho(0)$ as a function of $(M/M_{\rm sat})^2$ at 50 and 100 K. The inset zooms in at small applied fields.

values of Eu^{2+} ions in the localized limit (7 μ_B and 7.94 μ_B, respectively). The linear increase of magnetization towards saturation [Fig. 1(d)] further suggests the magnetic structure of our $EuZn_2As_2$ sample is simple A-AFM [9,10], as a nonlinear magnetization is observed in samples with a canted AFM structure [47].

Compared with a previous study [9], the magnitude of resistivity in our sample is several times larger, the upturn at low temperatures is more prominent, and the ground state is more insulating. To understand the origin of these discrepancies, we compare the Hall resistivity measured in our sample with similar measurements from Ref. [9], shown in Fig. 2(a). As can be seen, the Hall resistivity measurements indicate hole carriers in both cases, although the carrier density in our sample is several times smaller.

These observations suggest that stoichiometric $EuZn_2As_2$ is likely a narrow-gap semiconductor, and inadvertent hole-doping plays a key role in determining the transport properties in real materials. The hole-doping may be associated with defects that could facilitate the formation of magnetic polarons, which was invoked to explain the negative MR in some Eu-based materials [11,12]. To test whether such a scenario applies to $EuZn_2As_2$, in which case $[\rho(B) - \rho(0)]/\rho(0)$ and $(M/M_{\rm sat})^2$ are expected to scale linearly at low fields in the Majumdar-Littlewood model [54,55], we plot $[\rho(B) - \rho(0)]/\rho(0)$ at two temperatures as a function of $(M/M_{\rm sat})^2$ in Fig. 2(b). The absence of a linear behavior at both 50 and 100 K suggests magnetic polarons do not play a major role in the MR of $EuZn_2As_2$ at these temperatures. For lower temperatures, the M-shaped behavior of $\rho(B)$ prohibits a similar analysis, and probes such as scanning tunneling microscopy may be able to clarify whether magnetic polarons play a role [56].

It is interesting to note that like the carrier concentration, the magnetic ground state of $EuZn_2As_2$ can vary based on the synthesis protocol. In addition to the simple A-AFM magnetic structure [9], $EuZn_2As_2$ with spin-canted AFM structures that lead to a topological Hall effect have been reported [46,47]. Similarly, A-AFM, FM, and spin-canted structures have been reported in $EuCd_2As_2$ [36,57–59]. Taken together, these works reveal that nearly degenerate and highly tunable magnetic ground states are common to $EuZn_2As_2$ and $EuCd_2As_2$.

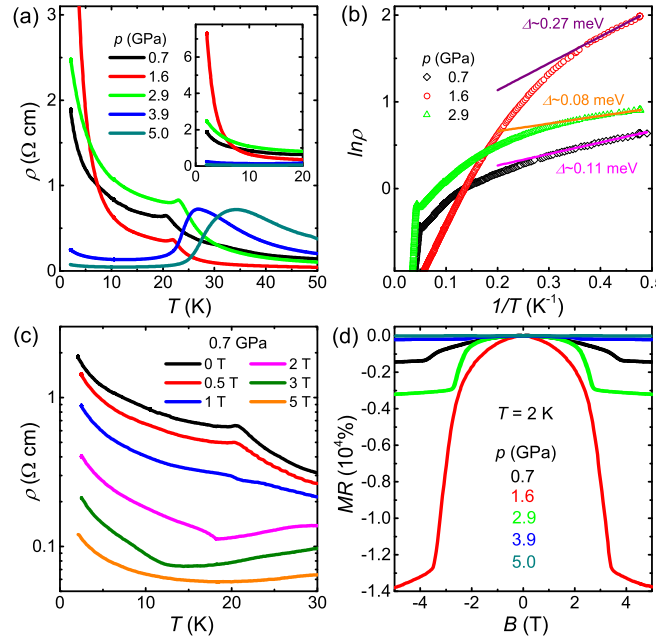

FIG. 3. Resistivity of $EuZn_2As_2$ at relatively low pressures. (a) $\rho(T)$ below 50 K, the inset zooms in around low temperatures. (b) ln ρ as a function of $1/T$, fit to an activated behavior $\rho \propto e^{\Delta/k_BT}$, where Δ is the activation energy. (c) $\rho(T)$ at 0.7 GPa, and under various applied magnetic fields. (d) MR $= [\rho(B) - \rho(0)]/\rho(B)$ at 2 K, compared for various pressures.

B. Electrical resistivity measurements under pressure

Electrical resistivity measurements were carried out for $EuZn_2As_2$ at various pressures, with the results shown in Figs. 3–5. At a relatively small pressure of 0.7 GPa, $\rho(T)$ at low temperatures become enhanced relative to ambient pressure, the insulating behavior manifests right below T_N, and the signature associated with the magnetic transition becomes a kink rather than the sharp peak at ambient pressure. These behaviors all point to $EuZn_2As_2$ becoming more insulating upon applying pressure. To confirm that the AFM state at ambient pressure persists in the more insulating state at 0.7 GPa, the evolution of $\rho(T)$ were measured under various magnetic fields, shown in Fig. 3(c). As can be seen, the kink associated with the magnetic transition moves to lower temperatures with increasing field, similar to the behavior at ambient pressure, which suggests that the magnetic structure remains AFM.

Upon further increasing pressure, we find the insulating state persists up to 2.9 GPa, and the most insulating behavior is observed at 1.6 GPa, with $\rho(2\,\text{K})$ exceeding 7 Ω cm. Values of the activation gap Δ for the insulating ground state are extracted by Arrhenius fitting $\rho(T) \propto e^{\Delta/k_BT}$ (k_B is the Boltzmann constant), indicated by solid lines in the plot of ln ρ against $1/T$ [Fig. 3(b)], with the maximum fit value of $\Delta \sim 0.27$ meV obtained at 1.6 GPa. We note that the resistivity $\rho(T)$ can also be captured by the variable-range hopping model $\rho(T) \propto e^{(T^*/T)^{1/4}}$, and the resulting Mott temperature T^* exhibits a qualitatively similar pressure dependence as the activation gap Δ.

Concomitant with $\rho(T)$ being the most insulating at 1.6 GPa, the MR, which is defined as $[\rho(B) - \rho(0)]/\rho(B)$,

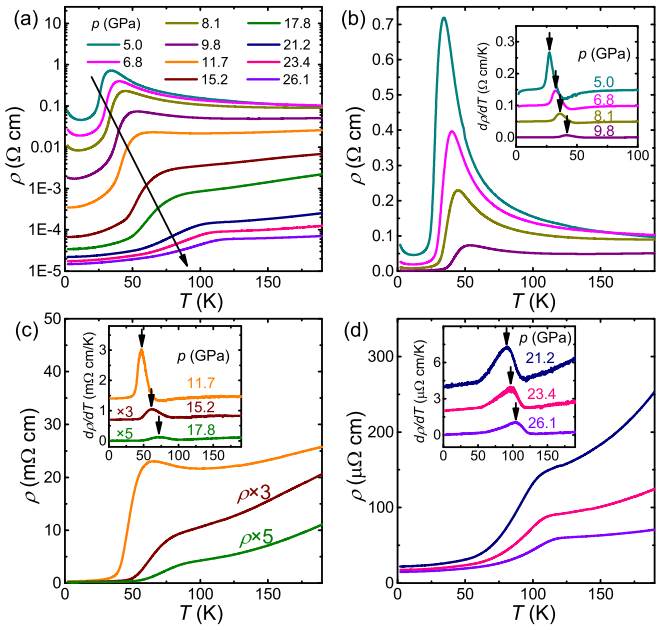

FIG. 4. (a) $\rho(T)$ at pressures from 5.0 to 26.1 GPa, plotted in log scale. (b) $\rho(T)$ at pressures from 5.0 to 9.8 GPa, (c) 11.7 to 17.8 GPa, and (d) 21.2 to 26.1 GPa, plotted in linear scales. The insets display $d\rho(T)/dT$, with data shifted vertically for clarity. The black arrows mark local maxima in $d\rho(T)/dT$, which we identify as magnetic transition temperatures.

also becomes dramatically enhanced and reaches a maximum over $1.4 \times 10^4\%$ at $B = 5$ T and $T = 2$ K [Fig. 3(d)]. The observation of MR being maximized at a pressure with the most insulating ground state (also the largest activation gap) suggests the CMR results from an insulator-metal transition driven by spin polarization due to the applied field. Such a scenario was also proposed to account for the CMR within the insulating dome of $EuCd_2As_2$ between ~1.0 and ~2.0 GPa [35].

Increasing pressure to 3.9 GPa, $\rho(T)$ upon cooling displays a rapid decrease after a broad hump [Fig. 3(a)], indicating a metallic ground state. Correspondingly, the MR at $T = 2$ K becomes much smaller compared to 1.6 or 2.9 GPa [Fig. 3(d)]. At 5.0 GPa, $EuZn_2As_2$ becomes more metallic with an even

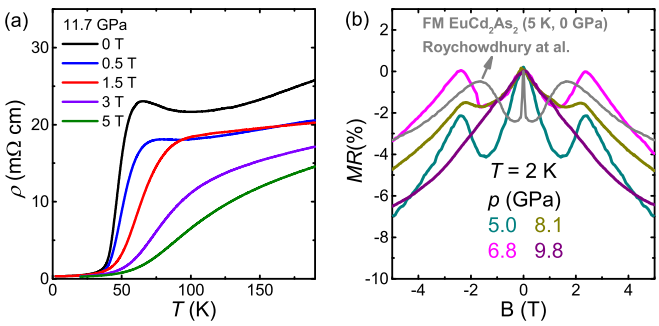

FIG. 5. (a) $\rho(T)$ at 11.7 GPa under various c-axis fields. (b) Field dependence of MR at 2 K and pressures from 5.0 to 9.8 GPa compared with the MR of FM $EuCd_2As_2$ at 5 K and ambient pressure from Ref. [58].

smaller MR at 2 K. These results evidence a pressure-induced insulator-metal transition around p_c, which occurs between 2.9 and 3.9 GPa, and further increase of pressure leads to better metallicity.

To investigate how this metallic state evolves at higher pressures, measurements of the electrical transport in $EuZn_2As_2$ were carried out for pressures up to 26.1 GPa, with results shown in Figs. 4 and 5. With increasing pressure, the hump feature in $\rho(T)$ gradually shifts to higher temperatures, and the resistivity decreases overall. For example, $\rho(2\,\mathrm{K})$ at 26.1 GPa is over 3 orders of magnitude smaller than that at 5.0 GPa [Fig. 4(a), note the log scale of the vertical axis]. Through such a metallization process with increasing pressure, $EuZn_2As_2$ changes from a bad metal with $\rho(2\,\mathrm{K}) \approx 75\,\mathrm{m\Omega\,cm}$ at 5.0 GPa, to a good metal with $\rho(2\,\mathrm{K}) \approx 15\,\mu\Omega\,\mathrm{cm}$ at 26.1 GPa. We note that while the magnetic transition appears to broaden significantly with pressure in Fig. 4(a), the same data plotted in linear scale reveal that the transitions remain reasonably sharp [Figs. 4(b)–4(d)], and the transition temperatures are determined from the local maxima in $d\rho(T)/dT$ [insets in Figs. 4(b)–4(d)].

Similar to $EuZn_2As_2$, a pressure-induced insulator-metal transition was observed in $EuCd_2As_2$ at ≈2.0 GPa and is accompanied by a change of the magnetic state from A-AFM to FM (or FM-like) [35,60–62]. This raises the question of whether a similar change of the magnetic state occurs in $EuZn_2As_2$, as its ground state transitions from an insulator to a metal with increasing pressure. Given the measurements in Fig. 3(c) already provide evidence that the insulating state in $EuZn_2As_2$ is AFM, we further carried out resistivity measurements under various magnetic fields at 11.7 GPa [Fig. 5(a)] to probe the magnetic state associated with the pressure-induced metallic phase of $EuZn_2As_2$. As can be seen, the magnetic transition shifts from ≈50 K to higher temperatures and broadens with increasing field, suggesting that the metallic ground state exhibits FM (or FM-like) order.

To further shed light on the magnetic ground state of $EuZn_2As_2$ above ~4 GPa, field dependence of the MR at several pressures between 5.0 and 9.8 GPa are shown in Fig. 5(b). The MR at these pressures differs qualitatively from those at lower pressures in two aspects: (1) the MR is smaller than those at low pressures by several orders of magnitude [Fig. 3(d)]; and (2) in contrast to the nearly monotonic field dependence at lower pressures [Fig. 3(d)], the MR at higher pressures exhibit a complex field dependence, resembling that of FM $EuCd_2As_2$ [gray line in Fig. 5(b)] [58]. Therefore both field dependence of the magnetic transition in Fig. 5(a) and the field dependence of MR in Fig. 5(b) suggest that a pressure-induced AFM-FM transition occurs in $EuZn_2As_2$ above ~4 GPa, similar to the pressure-induced AFM-FM transition in $EuCd_2As_2$ above ≈2.0 GPa [35,60].

C. First-principles calculations

First-principles calculations were carried out to gain insight on how the magnetic ground state and pressure affects the electrical transport properties of $EuZn_2As_2$. Figure 6(a) displays the ambient-pressure (0 GPa) electronic structure of $EuZn_2As_2$ for the A-AFM configuration with in-plane moments, which matches the experimentally determined

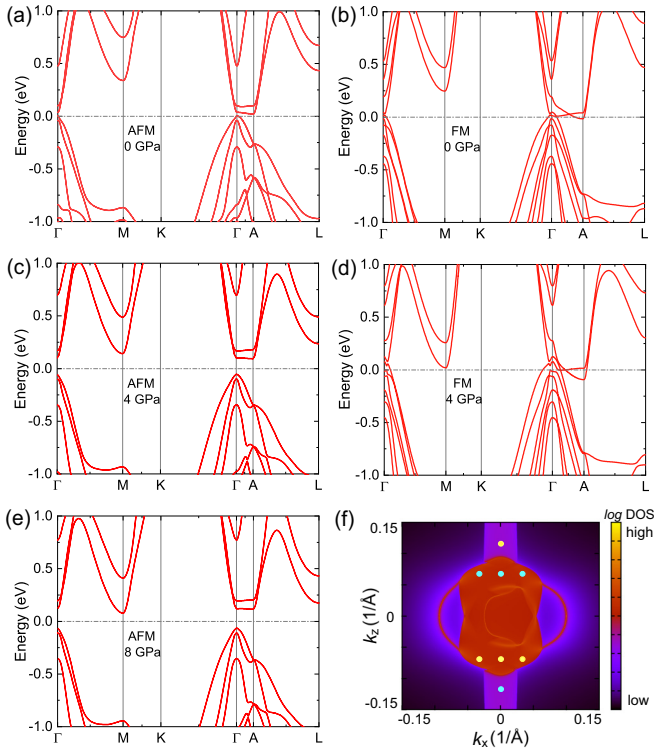

FIG. 6. First-principles calculations for $EuZn_2As_2$. Electronic structures for (a) the A-AFM state at 0 GPa, (b) the *c*-axis spin-polarized/FM state at 0 GPa. (c) and (d) respectively show the electronic structures of A-AFM and *c*-axis spin-polarized/FM $EuZn_2As_2$ at 4 GPa. (e) Electronic structure for the A-AFM state at 8 GPa. (f) The Weyl nodes with positive (yellow) and negative (cyan) chirality and Fermi arc surface states in the spin-polarized/FM state at 4 GPa.

magnetic structure [9,10,46]. The calculated electronic structure exhibits a narrow band gap between the valence and conduction bands, leading to insulating transport properties. Inadvertent doping is likely present in real materials, resulting in small sample-dependent carrier concentrations [Fig. 2(a)] and small activation gaps [Fig. 3(b)]. The semiconducting ground state of stoichiometric $EuZn_2As_2$, combined with a small hole carrier concentration, qualitatively account for the behaviors of $\rho(T)$ at ambient pressure [Fig. 1(a)].

Figure 6(b) displays the ambient-pressure band structure for the spin-polarized/FM configuration with moments along the *c* axis, which describes $EuZn_2As_2$ under a *c*-axis magnetic field (above the saturation field of ≈3.9 T). The calculated band gap closes in the spin-polarized/FM state, evidencing that the MR at ambient pressure results from an insulator-metal transition induced by the applied magnetic field. In this scenario, the weak upturn in $\rho(T)$ above the saturation field [5 T data in the inset of Fig. 1(a)] may result from scattering due to defects.

Figure 6(c) displays the band structure of AFM $EuZn_2As_2$ at 4 GPa, which is a trivial insulator similar to that at ambient pressure but with a larger charge gap. For the spin-polarized/FM state of $EuZn_2As_2$ at 4 GPa, a Weyl metal state is observed [Fig. 6(d)], with Weyl nodes located ∼5 meV above the Fermi level. Since Weyl fermions and topologically trivial electronic states both contribute to metallic conduction and the density of states at the Fermi level, $EuZn_2As_2$ is a "Weyl metal" [63,64]. Weyl nodes with different chirality and Fermi arc surface states at 4 GPa are shown in Fig. 6(f). Similar Weyl nodes are also found in Fig. 6(b), indicating that the spin-polarized/FM state at 0 GPa is also a Weyl metal.

Our calculations show the insulating gap in the A-AFM state and Weyl nodes in the spin-polarized/FM state persist from 0 to 4 GPa, suggesting that these features of $EuZn_2As_2$ are relatively robust against pressure for a given magnetically ordered state. This view is further supported by the persistence of an insulating state at 8 GPa, if the magnetic state remains A-AFM [Fig. 6(e)]. On the other hand, a transformation of the magnetic configuration from A-AFM to spin-polarized/FM at these pressures reconstructs the electronic structure, changing the system from a TrI to a Weyl metal.

These calculations suggest the insulating gap should increase until the applied pressure induces a change in the magnetic structure, beyond which point the insulating state becomes metallic. Experimentally, the observed activation gap Δ is smaller at 2.9 GPa compared to 1.6 GPa [Fig. 3(b)], and the activation gaps are overall much smaller than the calculated band gaps in Figs. 6(a) and 6(c). These discrepancies may result from the fact that $EuZn_2As_2$ samples are inadvertently hole doped [Fig. 2(a)], and the activation gap probes the energy difference between the acceptor level and the valence band top, rather than the band gap in the first-principles calculations.

IV. DISCUSSION

Based on the transport measurements under pressure, we construct the temperature-pressure phase diagram of $EuZn_2As_2$ [Fig. 7(a)], with the normalized resistivity $\rho(T)/\rho(290\,\mathrm{K})$ encoded in color and the magnetic transitions temperatures determined through the maxima in $d\rho(T)/dT$. At ambient and low pressures, the ground state is insulating AFM [inset of Figs. 1(a) and 3(c)], and T_N increases slightly with increasing pressure. Within the insulating phase, a CMR effect up to $1.4 \times 10^4\%$ is observed, which can be attributed to the topological phase transition from a TrI to a Weyl metal, based on the DFT calculations [Fig. 6]. Such a topological phase transition results from the polarization of Eu^{2+} moments, which leads to a significant reconstruction of the electronic structure. With increasing pressure, the ground state changes from an insulator to a metal at p_c between 2.9 and 3.9 GPa, and the CMR effect mostly disappears in the metallic phase.

Since spin polarization induces an insulator-metal transition in $EuZn_2As_2$, we propose that the pressure-induced insulator-metal transition in $EuZn_2As_2$ corresponds to a change of the magnetic ground state from AFM to FM (or FM-like). This view is supported by (1) the observation of experimental signatures for an AFM state at ambient pressure and 0.7 GPa [Figs. 1(a) and 3(c)] that evolve to FM-like at pressures above p_c [Fig. 5]; (2) DFT calculations show that AFM $EuZn_2As_2$ remains an insulator up to at least 8 GPa [Fig. 6(e)], a pressure at which $EuZn_2As_2$ is experimentally a metal [Fig. 4(a)]; and (3) the pressure-induced insulator-metal transition in $EuCd_2As_2$ is accompanied by an AFM-FM

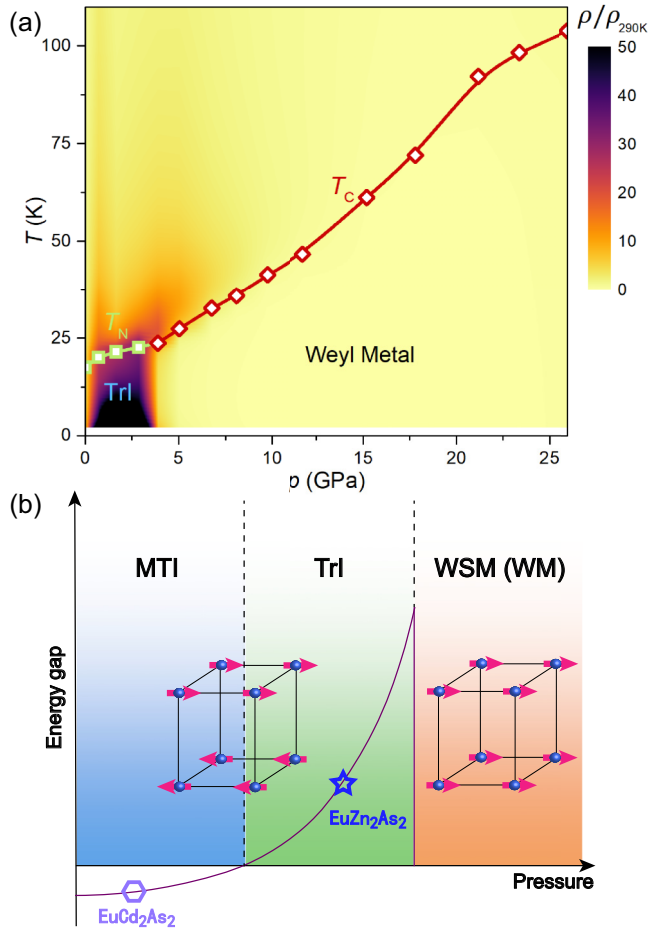

FIG. 7. (a) The temperature-pressure phase diagram of $EuZn_2As_2$ at zero field, where the values of the normalized resistivity are color-coded. The empty rectangles and diamonds respectively represent the Néel temperature T_N and Curie temperature T_C, determined from the local maxima in $d\rho/dT$, consistent with works on $EuCd_2As_2$ [35,60]. The solid lines are guides to the eyes. TrI represents a trivial insulator. (b) Unified schematic diagram for the ground states of $EuZn_2As_2$ and $EuCd_2As_2$ based on first-principles calculations, including a magnetic topological insulator (MTI), a trivial insulator (TrI), and a Weyl semimetal (WSM) or Weyl metal (WM) [35]. The solid line denotes the energy gap. The empty star and hexagon represent ambient-pressure $EuZn_2As_2$ and $EuCd_2As_2$, respectively.

transition [35,60]. Furthermore, the magnetic transition temperature increases with pressure at a larger rate beyond p_c [Fig. 7(a)], consistent with a change of the magnetic ground state occurring at p_c.

Our experiments and first-principles calculations reveal several features common to $EuZn_2As_2$ and $EuCd_2As_2$. Both systems exhibit an insulating state with A-AFM order [magnetic structure on the left of Fig. 7(b)], and the polarization of spins under an applied magnetic field leads to a CMR effect and a topological phase transition. Both systems exhibit a pressure-induced insulator-metal transition, likely concomitant with a change of the magnetic state from AFM to FM [magnetic structure on the right of Fig. 7(b)]. In contrast to $EuCd_2As_2$, which is likely an MTI at ambient pressure and becomes a TrI with the application of pressure, $EuZn_2As_2$ is already a TrI state at ambient pressure. These observations suggest that the ground states of $EuZn_2As_2$ and $EuCd_2As_2$ upon pressure tuning can be consistently understood, as depicted in Fig. 7(b). The reason for the absence of a MTI state in ambient-pressure $EuZn_2As_2$ is twofold. First, the smaller atomic radius of Zn relative to Cd effectively acts as chemical pressure, pushing $EuZn_2As_2$ towards the TrI phase. Second, the chemical pressure enhances electronic hopping and Zn exhibits weaker spin-orbit coupling relative to Cd, both acting to suppress band inversion necessary for a MTI phase.

While several mechanisms are proposed to account for CMR in Eu-based materials, the studies on $EuCd_2As_2$ and $EuZn_2As_2$ suggest that the mechanism in these materials is band reconstruction associated with the change in magnetic structure. We note the dominant CMR effect in $EuCd_2As_2$ and $EuZn_2As_2$ is qualitatively different from that reported in $EuCd_2P_2$ [8]. CMR in the former systems is mostly driven by field-induced changes in the magnetic structure and is maximized at lowest temperatures, whereas CMR in $EuCd_2P_2$ maximizes around the magnetic transition temperature and its origin is still being studied [7,8,13–15].

Since the CMR effects in $EuCd_2As_2$ and $EuZn_2As_2$ are associated with transitions from topologically trivial phases to nontrivial phases, topologically protected surface states are generated in the process. This raises the possibility of engineering tunable topologically protected surface states, which are particularly interesting in flake or film samples, where electrical transport due to surface states becomes more important.

In summary, our work on $EuZn_2As_2$ reveals it to be an AFM insulator at pressures below p_c (occurring between 2.9 and 3.9 GPa), with a maximum CMR of over 10^4%. Upon applying pressures beyond p_c, $EuZn_2As_2$ goes through an insulator-metal transition, likely resulting from a change of the magnetic state from A-type AFM to FM. The corresponding reconstruction of electronic bands results in a topological phase transition, from a trivial insulator phase to a Weyl metal phase. These results in $EuZn_2As_2$ are similar to observations in $EuCd_2As_2$ and suggest a unified understanding for the pressure-tuned evolution of their ground states and electrical transport. The CMR in both materials results from an insulator-metal transition driven by the polarization of Eu^{2+} ions, with the corresponding electronic structure simultaneously changing from topologically trivial to nontrivial. Our findings highlight Eu-based materials as promising platforms for the discovery of highly tunable magnetic topological matter and functional properties that arise from topological phase transitions.

ACKNOWLEDGMENTS

We acknowledge helpful discussions with F. Steglich, M. Shi, W. Zhu, Y. Liu, Z. Wang, M. Smidman, and H. Zhang. This work was supported by the Pioneer and Leading Goose R&D Program of Zhejiang (2022SDXHDX0005), the National Key R&D Program of China (No. 2022YFA1402200), the Key R&D Program of Zhejiang Province, China (Grant No. 2021C01002), and the National Natural Science Foundation of China (No. 11974306 and No. 12034017).

[1] Y. Tokura, Critical features of colossal magnetoresistive manganites, Rep. Prog. Phys. **69**, 797 (2006).

[2] A. P. Ramirez, Colossal magnetoresistance, J. Phys.: Condens. Matter **9**, 8171 (1997).

[3] Z. L. Sun, A. F. Wang, H. M. Mu, H. H. Wang, Z. F. Wang, T. Wu, Z. Y. Wang, X. Y. Zhou, and X. H. Chen, Field-induced metal-to-insulator transition and colossal anisotropic magnetoresistance in a nearly Dirac material $EuMnSb_2$, npj Quantum Mater. **6**, 94 (2021).

[4] J. Yin, C. Wu, L. Li, J. Yu, H. Sun, B. Shen, B. A. Frandsen, D.-X. Yao, and M. Wang, Large negative magnetoresistance in the antiferromagnetic rare-earth dichalcogenide $EuTe_2$, Phys. Rev. Mater. **4**, 013405 (2020).

[5] G. Wang, G. Chang, H. Zhou, W. Ma, H. Lin, M. Z. Hasan, S.-Y. Xu, and S. Jia, Field-induced metal-insulator transition in β-EuP_3, Chin. Phys. Lett. **37**, 107501 (2020).

[6] H. Yang, Q. Liu, Z. Liao, L. Si, P. Jiang, X. Liu, Y. Guo, J. Yin, M. Wang, Z. Sheng, Y. Zhao, Z. Wang, Z. Zhong, and R.-W. Li, Colossal angular magnetoresistance in the antiferromagnetic semiconductor $EuTe_2$, Phys. Rev. B **104**, 214419 (2021).

[7] H. Zhang, F. Du, X. Zheng, S. Luo, Y. Wu, H. Zheng, S. Cui, Z. Sun, Z. Liu, D. Shen, M. Smidman, Y. Song, M. Shi, Z. Zhong, C. Cao, H. Yuan, and Y. Liu, Electronic band reconstruction across the insulator-metal transition in colossal magnetoresistive $EuCd_2P_2$, arXiv:2308.16844.

[8] Z.-C. Wang, J. D. Rogers, X. Yao, R. Nichols, K. Atay, B. Xu, J. Franklin, I. Sochnikov, P. J. Ryan, D. Haskel, and F. Tafti, Colossal magnetoresistance without mixed valence in a layered phosphide crystal, Adv. Mater. **33**, 2005755 (2021).

[9] Z.-C. Wang, E. Been, J. Gaudet, G. M. A. Alqasseri, K. Fruhling, X. Yao, U. Stuhr, Q. Zhu, Z. Ren, Y. Cui, C. Jia, B. Moritz, S. Chowdhury, T. Devereaux, and F. Tafti, Anisotropy of the magnetic and transport properties of $EuZn_2As_2$, Phys. Rev. B **105**, 165122 (2022).

[10] J. Blawat, M. Marshall, J. Singleton, E. Feng, H. Cao, W. Xie, and R. Jin, Unusual electrical and magnetic properties in layered $EuZn_2As_2$, Adv. Quantum Technol. **5**, 2200012 (2022).

[11] Y. Zhang, K. Deng, X. Zhang, M. Wang, Y. Wang, C. Liu, J.-W. Mei, S. Kumar, E. F. Schwier, K. Shimada, C. Chen, and B. Shen, In-plane antiferromagnetic moments and magnetic polaron in the axion topological insulator candidate $EuIn_2As_2$, Phys. Rev. B **101**, 205126 (2020).

[12] P. Rosa, Y. Xu, M. Rahn, J. Souza, S. Kushwaha, L. Veiga, A. Bombardi, S. Thomas, M. Janoschek, E. Bauer, M. Chan, Z. Wang, J. Thompson, N. Harrison, P. Pagliuso, A. Bernevig, and F. Ronning, Colossal magnetoresistance in a nonsymmorphic antiferromagnetic insulator, npj Quantum Mater. **5**, 52 (2020).

[13] V. Sunko, Y. Sun, M. Vranas, C. C. Homes, C. Lee, E. Donoway, Z.-C. Wang, S. Balguri, M. B. Mahendru, A. Ruiz, B. Gunn, R. Basak, E. Schierle, E. Weschke, F. Tafti, A. Frano, and J. Orenstein, Spin-carrier coupling induced ferromagnetism and giant resistivity peak in $EuCd_2P_2$, Phys. Rev. B **107** 144404 (2023).

[14] C. C. Homes, Z.-C. Wang, K. Fruhling, and F. Tafti, Optical properties and carrier localization in the layered phosphide $EuCd_2P_2$, Phys. Rev. B **107**, 045106 (2023).

[15] B. Flebus, Magnetoresistance driven by the magnetic Berezinskii-Kosterlitz-Thouless transition, Phys. Rev. B **104**, L020408 (2021).

[16] E. Heinrich, T. Posske, and B. Flebus, Topological magnetic phase transition in Eu-based A-type antiferromagnets, Phys. Rev. B **106**, 214402 (2022).

[17] H. Watanabe, H. C. Po, and A. Vishwanath, Structure and topology of band structures in the 1651 magnetic space groups, Sci. Adv. **4**, eaat8685 (2018).

[18] Y. Xu, L. Elcoro, Z.-D. Song, B. J. Wieder, M. G. Vergniory, N. Regnault, Y. Chen, C. Felser, and B. A. Bernevig, High-throughput calculations of magnetic topological materials, Nature (London) **586**, 702 (2020).

[19] L. Elcoro, B. J. Wieder, Z. Song, Y. Xu, B. Bradlyn, and B. A. Bernevig, Magnetic topological quantum chemistry, Nat. Commun. **12**, 5965 (2021).

[20] B. A. Bernevig, C. Felser, and H. Beidenkopf, Progress and prospects in magnetic topological materials, Nature (London) **603**, 41 (2022).

[21] F. Tang and X. Wan, Exhaustive construction of effective models in 1651 magnetic space groups, Phys. Rev. B **104**, 085137 (2021).

[22] Z. Zhang, G.-B. Liu, Z.-M. Yu, S. A. Yang, and Y. Yao, Encyclopedia of emergent particles in type-IV magnetic space groups, Phys. Rev. B **105**, 104426 (2022).

[23] J. Yang, C. Fang, and Z.-X. Liu, Symmetry-protected nodal points and nodal lines in magnetic materials, Phys. Rev. B **103**, 245141 (2021).

[24] J. Zou, Z. He, and G. Xu, The study of magnetic topological semimetals by first principles calculations, npj Comput. Mater. **5**, 96 (2019).

[25] X. Wan, A. M. Turner, A. Vishwanath, and S. Y. Savrasov, Topological semimetal and Fermi-arc surface states in the electronic structure of pyrochlore iridates, Phys. Rev. B **83**, 205101 (2011).

[26] X.-P. Yao and G. Chen, $Pr_2Ir_2O_7$: When Luttinger semimetal meets Melko-Hertog-Gingras spin ice state, Phys. Rev. X **8**, 041039 (2018).

[27] G. Hua, S. Nie, Z. Song, R. Yu, G. Xu, and K. Yao, Dirac semimetal in type-IV magnetic space groups, Phys. Rev. B **98**, 201116(R) (2018).

[28] J.-R. Soh, F. de Juan, M. G. Vergniory, N. B. M. Schröter, M. C. Rahn, D. Y. Yan, J. Jiang, M. Bristow, P. Reiss, J. N. Blandy, Y. F. Guo, Y. G. Shi, T. K. Kim, A. McCollam, S. H. Simon, Y. Chen, A. I. Coldea, and A. T. Boothroyd, Ideal Weyl semimetal induced by magnetic exchange, Phys. Rev. B **100**, 201102(R) (2019).

[29] L.-L. Wang, N. H. Jo, B. Kuthanazhi, Y. Wu, R. J. McQueeney, A. Kaminski, and P. C. Canfield, Single pair of Weyl fermions in the half-metallic semimetal $EuCd_2As_2$, Phys. Rev. B **99**, 245147 (2019).

[30] J.-Z. Ma, S. M. Nie, C. J. Yi, J. Jandke, T. Shang, M. Y. Yao, M. Naamneh, L. Q. Yan, Y. Sun, A. Chikina, V. N. Strocov, M. Medarde, M. Song, Y.-M. Xiong, G. Xu, W. Wulfhekel, J. Mesot, M. Reticcioli, C. Franchini, C. Mudry *et al.*, Spin fluctuation induced Weyl semimetal state in the paramagnetic phase of $EuCd_2As_2$, Sci. Adv. **5**, eaaw4718 (2019).

[31] J. Ma, H. Wang, S. Nie, C. Yi, Y. Xu, H. Li, J. Jandke, W. Wulfhekel, Y. Huang, D. West, P. Richard, A. Chikina, V. N. Strocov, J. Mesot, H. Weng, S. Zhang, Y. Shi, T. Qian, M. Shi, and H. Ding, Emergence of nontrivial low-energy Dirac fermions in antiferromagnetic $EuCd_2As_2$, Adv. Mater. **32**, 1907565 (2020).

[32] H. Su, B. Gong, W. Shi, H. Yang, H. Wang, W. Xia, Z. Yu, P.-J. Guo, J. Wang, L. Ding, L. Xu, X. Li, X. Wang, Z. Zou, N. Yu, Z. Zhu, Y. Chen, Z. Liu, K. Liu, G. Li *et al.*, Magnetic exchange induced Weyl state in a semimetal $EuCd_2Sb_2$, APL Mater. **8**, 011109 (2020).

[33] F. Kabir, M. M. Hosen, F. C. Kabeer, A. Aperis, X. Ding, G. Dhakal, K. Dimitri, C. Sims, S. Regmi, L. Persaud, K. Gofryk, P. M. Oppeneer, D. Kaczorowski, and M. Neupane, Observation of multiple Dirac states in a magnetic topological material $EuMg_2Bi_2$, arXiv:1912.08645.

[34] M. Kondo, M. Ochi, R. Kurihara, A. Miyake, Y. Yamasaki, M. Tokunaga, H. Nakao, K. Kuroki, T. Kida, M. Hagiwara, H. Murakawa, N. Hanasaki, and H. Sakai, Field-tunable Weyl points and large anomalous Hall effects in degenerate magnetic semiconductor $EuMg_2Bi_2$, Phys. Rev. B **107**, L121112 (2023).

[35] F. Du, L. Yang, Z. Nie, N. Wu, Y. Li, S. Luo, Y. Chen, D. Su, M. Smidman, Y. Shi, C. Cao, F. Steglich, Y. Song, and H. Yuan, Consecutive topological phase transitions and colossal magnetoresistance in a magnetic topological semimetal, npj Quantum Mater. **7**, 65 (2022).

[36] M. C. Rahn, J.-R. Soh, S. Francoual, L. S. I. Veiga, J. Strempfer, J. Mardegan, D. Y. Yan, Y. F. Guo, Y. G. Shi, and A. T. Boothroyd, Coupling of magnetic order and charge transport in the candidate Dirac semimetal $EuCd_2As_2$, Phys. Rev. B **97**, 214422 (2018).

[37] H. P. Wang, D. S. Wu, Y. G. Shi, and N. L. Wang, Anisotropic transport and optical spectroscopy study on antiferromagnetic triangular lattice $EuCd_2As_2$: An interplay between magnetism and charge transport properties, Phys. Rev. B **94**, 045112 (2016).

[38] Y. Xu, L. Das, J. Z. Ma, C. J. Yi, S. M. Nie, Y. G. Shi, A. Tiwari, S. S. Tsirkin, T. Neupert, M. Medarde, M. Shi, J. Chang, and T. Shang, Unconventional transverse transport above and below the magnetic transition temperature in Weyl semimetal $EuCd_2As_2$, Phys. Rev. Lett. **126**, 076602 (2021).

[39] P. Klüfers, H. Neumann, A. Mewis, and H.-U. Schuster, AB_2X_2-verbindungen im $CaAl_2Si_2$-type, VIII [1], Z. Naturforschung B **35**, 1317 (1980).

[40] J.-R. Soh, C. Donnerer, K. M. Hughes, E. Schierle, E. Weschke, D. Prabhakaran, and A. T. Boothroyd, Magnetic and electronic structure of the layered rare-earth pnictide $EuCd_2Sb_2$, Phys. Rev. B **98**, 064419 (2018).

[41] V. K. Anand and D. C. Johnston, Metallic behavior induced by potassium doping of the trigonal antiferromagnetic insulator $EuMn_2As_2$, Phys. Rev. B **94**, 014431 (2016).

[42] T. Berry, V. J. Stewart, B. W. Y. Redemann, C. Lygouras, N. Varnava, D. Vanderbilt, and T. M. McQueen, A-type antiferromagnetic order in the Zintl-phase insulator $EuZn_2P_2$, Phys. Rev. B **106**, 054420 (2022).

[43] S. Krebber, M. Kopp, C. Garg, K. Kummer, J. Sichelschmidt, S. Schulz, G. Poelchen, M. Mende, A. V. Virovets, K. Warawa, M. D. Thomson, A. V. Tarasov, D. Y. Usachov, D. V. Vyalikh, H. G. Roskos, J. Müller, C. Krellner, and K. Kliemt, Colossal magnetoresistance in $EuZn_2P_2$ and its electronic and magnetic structure, Phys. Rev. B **108**, 045116 (2023).

[44] S. Pakhira, A. K. Kundu, F. Islam, M. A. Tanatar, T. Roy, T. Heitmann, T. Yilmaz, E. Vescovo, M. Tsujikawa, M. Shirai, R. Prozorov, D. Vaknin, and D. C. Johnston, Anisotropic magnetism and electronic structure of trigonal $EuAl_2Ge_2$ single crystals, Phys. Rev. B **107**, 134439 (2023).

[45] W. Bi, T. Culverhouse, Z. Nix, W. Xie, H.-J. Tien, T.-R. Chang, U. Dutta, J. Zhao, B. Lavina, E. E. Alp, D. Zhang, J. Xu, Y. Xiao, and Y. K. Vohra, Drastic enhancement of magnetic critical temperature and amorphization in topological magnet $EuSn_2P_2$ under pressure, npj Quantum Mater. **7**, 43 (2022).

[46] E. Yi, D. F. Zheng, F. Pan, H. Zhang, B. Wang, B. Chen, D. Wu, H. Liang, Z. X. Mei, H. Wu, S. A. Yang, P. Cheng, M. Wang, and B. Shen, Topological Hall effect driven by short-range magnetic order in $EuZn_2As_2$, Phys. Rev. B **107**, 035142 (2023).

[47] Z. Bukowski, D. Rybicki, M. Babij, J. Przewoźnik, Ł. Gondek, J. Żukrowski, and C. Kapusta, Canted antiferromagnetic order in $EuZn_2As_2$ single crystals, Sci. Rep. **12**, 14718 (2022).

[48] J. P. Perdew, K. Burke, and M. Ernzerhof, Generalized gradient approximation made simple, Phys. Rev. Lett. **77**, 3865 (1996).

[49] G. Kresse and J. Furthmüller, Efficient iterative schemes for ab initio total-energy calculations using a plane-wave basis set, Phys. Rev. B **54**, 11169 (1996).

[50] A. A. Mostofi, J. R. Yates, Y.-S. Lee, I. Souza, D. Vanderbilt, and N. Marzari, Wannier90: A tool for obtaining maximally-localised Wannier functions, Comput. Phys. Commun. **178**, 685 (2008).

[51] G.-X. Zhi, C. Xu, S.-Q. Wu, F. Ning, and C. Cao, WannSymm: A symmetry analysis code for Wannier orbitals, Comput. Phys. Commun. **271**, 108196 (2022).

[52] Q. Wu, S. Zhang, H.-F. Song, M. Troyer, and A. A. Soluyanov, WannierTools: An open-source software package for novel topological materials, Comput. Phys. Commun. **224**, 405 (2018).

[53] J. Blawat, S. Speer, J. Singleton, W. Xie, and R. Jin, Quantum-limit phenomena and bandstructure in the magnetic topological semimetal $EuZn_2As_2$, arXiv:2304.12426.

[54] P. Majumdar and P. B. Littlewood, Dependence of magnetoresistivity on charge-carrier density in metallic ferromagnets and doped magnetic semiconductors, Nature (London) **395**, 479 (1998).

[55] W. Shon, J.-S. Rhyee, Y. Jin, and S.-J. Kim, Magnetic polaron and unconventional magnetotransport properties of the single-crystalline compound $EuBiTe_3$, Phys. Rev. B **100**, 024433 (2019).

[56] M. Pohlit, S. Rößler, Y. Ohno, H. Ohno, S. von Molnár, Z. Fisk, J. Müller, and S. Wirth, Evidence for ferromagnetic clusters in the colossal-magnetoresistance material EuB_6, Phys. Rev. Lett. **120**, 257201 (2018).

[57] N. H. Jo, B. Kuthanazhi, Y. Wu, E. Timmons, T.-H. Kim, L. Zhou, L.-L. Wang, B. G. Ueland, A. Palasyuk, D. H. Ryan, R. J. McQueeney, K. Lee, B. Schrunk, A. A. Burkov, R. Prozorov, S. L. Bud'ko, A. Kaminski, and P. C. Canfield, Manipulating magnetism in the topological semimetal $EuCd_2As_2$, Phys. Rev. B **101**, 140402(R) (2020).

[58] S. Roychowdhury, M. Yao, K. Samanta, S. Bae, D. Chen, S. Ju, A. Raghavan, N. Kumar, P. Constantinou, S. N. Guin, N. C. Plumb, M. Romanelli, H. Borrmann, M. G. Vergniory, V. N. Strocov, V. Madhavan, C. Shekhar, and C. Felser, Anomalous Hall conductivity and Nernst effect of the ideal Weyl semimetallic ferromagnet $EuCd_2As_2$, Adv. Sci. **10**, 2207121 (2023).

[59] K. M. Taddei, L. Yin, L. D. Sanjeewa, Y. Li, J. Xing, C. de la Cruz, D. Phelan, A. S. Sefat, and D. S. Parker, Single pair of Weyl nodes in the spin-canted structure of $EuCd_2As_2$, Phys. Rev. B **105**, L140401 (2022).

[60] E. Gati, S. L. Bud'ko, L.-L. Wang, A. Valadkhani, R. Gupta, B. Kuthanazhi, L. Xiang, J. M. Wilde, A. Sapkota, Z. Guguchia, R. Khasanov, R. Valentí, and P. C. Canfield, Pressure-induced ferromagnetism in the topological semimetal $EuCd_2As_2$, Phys. Rev. B **104**, 155124 (2021).

[61] Z. Yu, X. Chen, W. Xia, N. Wang, X. Lv, D. Wu, W. Wu, Z. Liu, J. Zhao, M. Li, S. Li, X. Li, Z. Dong, C. Zhou, L. Zhang, X. Wang, N. Yu, Z. Zou, J. Luo, J. Cheng *et al.*, Structure, magnetotransport, and theoretical study on the layered antiferromagnet topological phase $EuCd_2As_2$ under high pressure, Adv. Quantum Technol. **6**, 2200128 (2023).

[62] G. C. Jose, K. Burrage, J. L. G. Jimenez, W. Xie, B. Lavina, J. Zhao, E. E. Alp, D. Zhang, Y. Xiao, Y. K. Vohra, and W. Bi, Evolution of magnetism, valence, and crystal lattice in $EuCd_2As_2$ under pressure, Phys. Rev. B **107**, 245121 (2023).

[63] A. Burkov, Weyl metals, Annu. Rev. Condens. Matter Phys. **9**, 359 (2018).

[64] Y. Yang, F. Yu, X. Wen, Z. Gui, Y. Zhang, F. Zhan, R. Wang, J. Ying, and X. Chen, Pressure-induced transition from a Mott insulator to a ferromagnetic Weyl metal in $La_2O_3Fe_2Se_2$, Nat. Commun. **14**, 2260 (2023).